J Nanopart Res (2015) 17:152
DOI 10.1007/s11051-015-2967-8

RESEARCH PAPER

Plasma synthesis of titanium nitride, carbide and carbonitride nanoparticles by means of reactive anodic arc evaporation from solid titanium

D. Kiesler · T. Bastuck · R. Theissmann · F. E. Kruis

Received: 17 June 2014 / Accepted: 13 March 2015 / Published online: 20 March 2015
© Springer Science+Business Media Dordrecht 2015

Abstract Plasma methods using the direct evaporation of a transition metal are well suited for the cost-efficient production of ceramic nanoparticles. In this paper, we report on the development of a simple setup for the production of titanium-ceramics by reactive anodic arc evaporation and the characterization of the aerosol as well as the nanopowder. It is the first report on TiC_XN_{1-X} synthesis in a simple anodic arc plasma. By means of extensive variations of the gas composition, it is shown that the composition of the particles can be tuned from titanium nitride over a titanium carbonitride phase (TiC_XN_{1-X}) to titanium carbide as proven by XRD data. The composition of the plasma gas especially a very low concentration of hydrocarbons around 0.2 % of the total plasma gas is crucial to tune the composition and to avoid the formation of free carbon. Examination of the particles by HR-TEM shows that the material consists mostly of cubic single crystalline particles with mean sizes between 8 and 27 nm.

D. Kiesler (✉) · T. Bastuck · R. Theissmann · F. E. Kruis
Institute of Technology for Nanostructures (NST) and Center for Nanointegration Duisburg-Essen (CENIDE), University of Duisburg-Essen, Bismarckstr. 81, 47057 Duisburg, Germany
e-mail: dennis.kiesler@uni-due.de

T. Bastuck
Federal-Mogul Burscheid GmbH, Rings & Liners, Buergermeister-Schmidt-Str. 17, 51399 Burscheid, Germany

Keywords Anodic arc · Plasma synthesis · Ceramic nanopowder · Aerosol synthesis · TiC titaniumcarbide · TiN titaniumnitride · TiCN titaniumcarbonitride

Introduction

Nanoparticulate nitride and carbide ceramic materials are attractive materials due to their improved sinterability compared to μm-sized particles (Ishigaki et al. 1995). They can be also used as a disperse phase to change the crystalline structure and properties of continuous solid materials (Thompson and Harmer 2011) or polymers like PET for food packaging (EFSA Panel on food contact materials enzymes (CEF) 2012). Especially titanium carbides and nitrides nanoparticles are often applied in nanoparticle-reinforced coatings, often as cermet-composites, e.g., in cobalt for wear-resistent coatings and cutting-tools (Guu et al. 1997; Manoj Kumar et al. 2008). Although titanium carbonitride has potentially attractive properties such as increased hardness, it is less often applied than the pure nitrides and carbides because its synthesis is more complicated and in nanoparticulate form the material is scarcely reported.

For the synthesis of TiN and TiC, reactive evaporation of Ti in low-pressure nitrogen either by ion or electron beam (Iwama et al. 1982; Ikegami et al. 2003; Yatsui et al. 1997) or chemical reactions of Ti-precursors initiated by microwave or infrared

radiation (Leconte et al. 2006; Alexandrescu et al. 1997; Mehta et al. 1991) can be applied. More often, high-temperature plasma synthesis methods are used. These can be classified according to plasma torches, both DC nontransferred arc and RF plasma torches, or DC anode evaporation, also known as transferred arc (Young and Pfender 1985; Pfender 1999). In a plasma torch, a plasma is created without evaporation of the torch material by applying high flow rates of the plasma-forming gas. The solid surfaces like the gas inlets and electrodes or the quartz tube have to be cooled to minimize erosion of the torch. The plasma gas is heated by means of a DC arc between a tungsten needle and a nozzle or by means of an inductively coupled plasma using an RF coil outside the quartz tube. The metal to be evaporated can be fed into the plasma either in form of an aerosolized powder or a gaseous metal precursor such as a metal chloride. In a transferred arc, the arc strikes directly on the material to be evaporated which acts as anode. The anode can be a solid rod when the temperature can be controlled such that enough material evaporates but the rod does not melt, but more often the metal is placed in a conducting crucible, e.g., a graphite crucible or a water-cooled copper crucible. The cathode is a non evaporating tungsten needle, placed in a short distance to the anode. The high temperatures reached in the thermal plasma lead to a fast reaction of the vaporized metal with reactants such as CH_4, NH_3, or N_2.

In recent times, in addition to TiN and TiC the titanium carbonitrides have attracted considerable interest due to improved physical properties such as larger hardness and the possibility to tailor the thermal conductivity between the very high values for TiN and the very low ones for TiC (Jhi et al. 1999; Yang et al. 2000). However, a controlled synthesis of the carbonitrides has proved to be very challenging. Synthesis methods reported until now are exothermic solid-state reactions at high temperatures between Ti or TiO_2 with graphite powder or (CN)-precursor in N_2 (Li et al. 2009; Monteverde et al. 2001; Seplyarskii et al. 2011; Mu et al. 2011; Mondal et al. 2008; Yeh and Chen 2005), autoclave methods where $TiCl_4$ and a reactants such as NaN_3 and CaC_2 or $C_3N_3Cl_3$ and Na react at temperatures below 1000 °C (Feng and Shi 2005; Shen et al. 2002; Lee et al. 2007; Zhang et al. 2008), high-intensity milling (Yin et al. 2009), and plasma methods. In Table 1, an overview is given of plasma processes reported in literature producing

Table 1 Plasma synthesis of TiCN nanoparticles, sorted by plasma generation method

Plasma method and parameters	Plasma gas	Reactants	Product	Reference
DC plasma torch 10 kW, 1 Atm	Ar 20 slm	CH_4 1.2-2.0 slm or N_2 1.2-2.0 slm Ti/TiO_2 powder	TiC or TiN [XRD], 10–30 nm [STEM]	Mitrofanov et al. (1981)
DC plasma torch 25 kW, 1 Atm	Air	$TiCl_4$ CH_4 N_2	TiCN [XRD], 16–120 nm [BET]	Alekseev et al. (1999)
RF plasma torch 100 kW @ 5.28 MHz, 1 Atm	N_2 140 slm	Ti powder, 20–40 µm, 15–20 g/min C_nH_m + NH_3	$TiC_{0.3}N_{0.7}$–$TiC_{0.7}N_{0.3}$ [XRD], 30 nm [BET]	Grabis and Zalite (2005)
RF Plasma Torch 35 kW @ 13.56 MHz, 1 Atm	Ar + H_2 86 slm sheath Ar 9.5 slm carrier	TiCN powder (1.4 µm) 2 g/min	TiCN [TEM–EELS], <30 nm [TEM]	Leparoux et al. (2008)

TiCN-based ceramic nanoparticles. From these methods, only the plasma synthesis method and the autoclave method yield the carbonitrides in the form of nanopowder. Solid-state reactions lead only to nanopowder when the Ti or TiO_2 starting powder is already in form of nanopowder (Li et al. 2009; Monteverde et al. 2001), whereas high-intensity milling leads to a nanocrystalline product but not to a nanopowder (Yin et al. 2009). In comparison, the plasma synthesis method is advantageous because no extensive purification steps have to be performed and it can be scaled-up easily. However, TiO_2 micropowder did not form TiCN but only TiC when mixed with CH_4 and N_2 in a DC plasma torch (Mitrofanov et al. 1981), probably due to carbon excess in the reactants. Plasma synthesis of titanium carbonitride from $TiCl_4$ and methane by a 25-kW DC plasma torch with air as plasma gas was successful due to the presence of oxygen which reduced the free carbon content, however, resulting in some oxygen contamination of the powder (Alekseev et al. 1999). TiCN particles with a mean diameter around 30 nm having a low oxygen and low free carbon content have been reported for the first time by Grabis et al. (Grabis and Zalite 2005). Here, single-phase TiCN is produced inside a 100-kW RF plasma torch when feeding micrometer-sized titanium- or titaniumhydride-powder in a nitrogen plasma, when a hydrocarbon or a hydrocarbon-ammonia mixture is injected into the plasma at a precise to define distances behind the powder injection. In a simpler plasma process (Leparoux et al. 2008) single-phase TiCN is produced using a 30-kW RF plasma torch by converting micrometer-sized TiCN powder into TiCN nanopowder in an Ar or Ar/H_2 atmosphere. With the DC anode evaporation method used in our work, only the production of pure TiC (Ishizaki et al. 1989; Jiao and Seraphin 1998) or pure TiN (Inoue et al. 1992; Mahoney and Andres 1995), but not of TiCN nanoparticles is reported.

In this work, a synthesis process is developed which is compatible with a PVD coating system, with the final goal of incorporating directly the freshly synthesized ceramic nanoparticles in a growing PVD film for tribological applications. Thus requiring a constant production rate over an extended time period (several hours) and which does not allow the use of corrosive or expensive chemical precursors. For the continuous generation of gas-carried nanoparticles based on a metal having a low vapor pressure and requiring high reaction temperatures to form carbides and/or nitrides, a plasma synthesis process is well suited. DC anode evaporation is the most suitable process compatible with a PVD setup because no large gas flow is necessary for stabilization of the plasma, and a low-cost TIG welder can be used as electrical power supply. Furthermore, special emphasis is placed on optimizing the synthesis process toward the controlled formation of titanium carbonitride.

Experimental

Reactor configuration

Contrary to prior plasma synthesis of TiC or TiN where a crucible containing liquid Ti was used, a solid 6 mm diameter Ti electrode is used as anode. This avoids contamination of the product with the crucible material and allows a flexible positioning inside the reactor, contrary to a crucible which allows only one position. The reactor is assembled from standard vacuum components (ISO-KF 40), in order to ensure an oxygen-free atmosphere to avoid the formation of oxidized particles. The vacuum components also allow a rapid modification of the reactor configuration. The use of a solid electrode requires an accurate positioning by means of a micrometer drive as well as a high-voltage, high-current vacuum feedthrough.

The flexible design allows multiple configurations to be tested. First, a horizontal electrode arrangement was tested. Using a W cathode instead of a Ti cathode leads to a more stable plasma because the cathodic hot spot necessary for electrode emission is present on the W electrode without resulting in its melting. However, the arc is stable less than 1 h and the arc length is difficult to control. Placing the electrodes vertically with the Ti anode on the top position and the W cathode below leads to the same problems. The final configuration tested (Fig. 1) applies a Ti anode mounted horizontally and a W cathode placed at 90°-below. This results in the Ti electrode being placed in the plasma stabilized by buoyancy. The plasma attachment is either at the bottom or the top of the Ti electrode but does not move toward the electrode holder. This arrangement is stable for many hours and is therefore selected as optimal configuration for the remaining part of this work. Two different arc modes due to the cathode spot position and thus

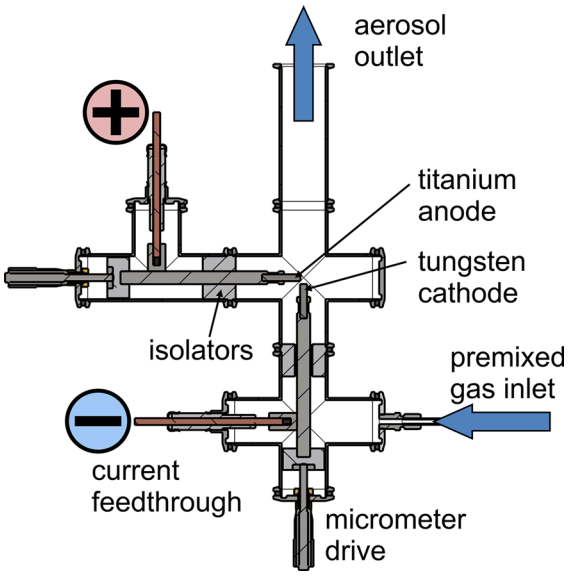

Fig. 1 Optimal reactor configuration: 90° design (*brown*: copper, current feedthrough connected to power source; *dark gray*: stainless steel parts, walls, and electrode holder; *light gray*: insulator parts; *black*: O-ring seals). The cathode (−) is a W electrode whereas the anode (+) is Ti. The *blue arrows* indicate gas inlet and aerosol outlet. (Color figure online)

different effective arc lengths can be observed. A long flame-like mode emerged out of the electrode gap having more than 10 mm arc length and an arc voltage between 20 and 30 V but is not well controllable. The other mode is the much more stable short mode, with only a few millimeters of arc length inside the gap and an arc voltage between 8 and 15 V. In this work, the short mode has been applied by tuning of the gap distance when the arc switched to the flame-like mode.

For all following experiments concerning production rate and composition, an improved chamber is used. It is based on a DN ISO 160 K tube having a length of 138 mm with four DN ISO 40 KF flanges welded at its circumference. A larger diameter is used because of the larger wall to plasma distance and a better heat dissipation. A double-walled construction allowed a continuous cooling with water. This final reactor design with the larger chamber can be seen in Fig. 2 (experimental setup) on the left. As in the first design, the electrode holder assembly combines the electrode positioning by means of a micrometer drive as well as a high-voltage high-current vacuum feedthrough. These two functions have to be uncoupled due to lack of a combined mechanical and electrical feedthrough. This is done by means of a vacuum-tee containing a stainless steel rod centered by a cylindrical piece of isolator material (MACOR) at the inlet to the reactor chamber. This rod is positioned by a micrometer having a range of 25 mm (07MAM704, CVI Melles Griot, Albuquerque, NM, USA) screwed in a KF40 flange and sealed by means of two O-rings from FKM. The rod is connected to the micrometer via an isolator and connected to a commercial current feedthrough (12 kV, 150 A) by

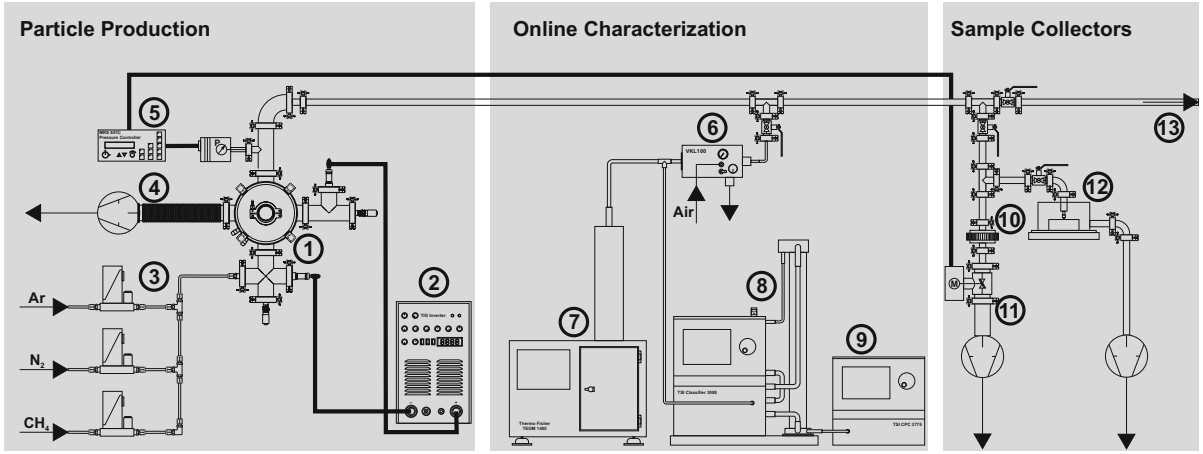

Fig. 2 Experimental setup. The particle production unit is composed of the reactor (*1*), the power supply (*2*), mass flow controllers (*3*), a vacuum pump for evacuation prior to synthesis (*4*), and a vacuum control unit (*5*). Online particle characterization is performed by means of a 1:100 diluter (*6*), a TEOM measuring mass concentration (*7*), a DMA with control unit (*8*), and a condensation particle counter (*9*). The product flow is led toward the PVD reactor (*13*), samples can be taken by means of a filter for gravimetric analysis and XRD (*10*). A pump regulated by means of a butterfly valve (*11*) allows to keep the process pressure constant. TEM grids are covered with particle samples by means of low-pressure impaction (*12*)

means of a spring contact. At the reactor bottom, using a vacuum cross for the 8 mm diameter W cathode instead of a vacuum tee allows to connect a gas inlet port and supplying the centering isolator with 4 holes with 2 mm diameter allows to co-flow a gas around the electrode. The two remaining KF40 ports are used as product flow outlet at the top and as connection to the vacuum pump.

Experimental setup and procedure

The experimental setup in use can be divided into three parts, namely particle production, online characterization, and sample collection (Fig. 2). The particle production unit contains the reactor and a power supply which is a commercial TIG welder (Klimag WIG200P, Schweißtechnik Klinger, Gladbeck, Germany) based on an IGBT inverter offering a regulated current between 5 and 200 A. The current was kept constant to 20 A for all the experiments shown in this work. The power supply can maintain the current as long as the arc voltage is below 30 V. A built-in high-frequency, high-voltage spark igniter allows the ignition without the need of the electrodes to touch each other. The gas in the reactor chamber is controlled by three thermal mass flow controllers (El-Flow, Bronckhorst, Ruurlo, Netherlands) with a maximum flowrate of 10 slm N_2, 10 slm Ar, and 3 sccm CH_4. The gases are premixed before entering the reactor. The gas inlet is connected at the bottom electrode holder assembly and leads to an upward flowing gas parallel to the tungsten cathode. The experiments are conducted at atmospheric pressure. On one port of the reactor chamber, a two-stage rotary vane pump having a pumping capacity of 65 m^3/h (Trivac D65B, Oerlikon Leybold Vacuum, Cologne, Gemany) is connected to allow the evacuation of the chamber down to 0.05 Pa in order to remove oxygen and other gaseous impurities before the process is started. Before every experiment, the chamber is evacuated by means of this pump to 0.5 Pa and is flooded with the reaction gas up to atmospheric pressure, this procedure is repeated three times. The pressure in the chamber is measured by a gas-type-independent capacitive absolute pressure gage (Baratron 626A, MKS, Andorer, MA, USA) and is connected to a pressure controller unit (615C, MKS) steering a butterfly valve in front of an additional rotary vane pump. This allows to maintain a constant pressure during the process even when a filter in the exhaust is increasingly loaded with particles. During the synthesis, a viewport placed in one of the ISO-K160 flanges allows the visual observation of the arc. The nitrogen or carbon atoms in the plasma gas can alter the Ti anode by forming TiCN on its surface. To obtain repeatable results, the Ti anode has to be exchanged with a new polished one, when the gas composition in the reactor is changed. The experimental parameters that are kept constant for all exeriments are summarized in Table 2.

Online characterization

The online characterization allows to measure the particle size distribution of the product aerosol and its mass concentration. Standard aerosol instruments can be used for this purpose but require dilution prior to measurements. This is performed by means of a 1:100 dilution stage based on the ejection principle (VKL 100, Palas, Karlsruhe, Germany) using particle-free pressurized air. This has the additional advantage that the different gas compositions of the product gas changing from pure argon to nitrogen and mixtures thereof do not disturb the measurements. A tapered element oscillating microbalance (TEOM model 1405, Thermo Scientific, Waltham, MA, USA, using an integration time of 1 min) is used to measure the mass concentration of the aerosol and enables the direct determination of the mass production rate of the reactor. The scanning mobility particle sizer (SMPS) is composed of a differential mobility analyzer (DMA, model 3081 and 3085, TSI, Minneapolis, MN, USA)

Table 2 Standard experimental conditions

System parameter	Value
Total gas flow rate Q_{tot} (Ar + N_2)	4.8 slm
Arc current I_{Arc}	20 A
Electrode gap	~2 mm
Cathode	Tungsten rod diam. 8 mm
Anode	Polished titanium rod diam. 6 mm

and condensation particle counter (CPC 3775, TSI). It allows the direct measurement of particle size distributions between 10 and 600 nm based on the particles' electrical mobility.

Sample preparation and characterization

The sample collection prepares samples for XRD and TEM. Two rotary vane pumps with a pumping capacity of 18 m^3/h (E2M18, Edwards, Crawley, UK) supply the necessary suction. A vacuum-tight stainless steel filter holder is mounted to collect samples for gravimetric measurements and XRD. The filters used are supported PTFE-membrane filters with a pore size of 5 µm and 40 mm in diameter (TE38, Whatman, Maidstone, UK). PTFE filters show good chemical stability and their hydrophobic nature minimizes moisture uptake. The large pore size of the filter was selected to have a low pressure drop over the filter and allowing longer sampling times which varied between 15 and 60 min. Tests with the particle counter show that after a few seconds a filter cake is formed and no nanoparticles penetrate the filter. These filters are also used to collect samples for X-ray diffraction (XRD) analysis to study the crystal structure and composition. The amorphous structure of the PTFE shows no diffraction peaks in the interesting range of between 30° and 130°. The measurement instrument is a powder diffractometer (X'Pert Pro, Panalytical, Almelo, Netherlands) using radiation with 0.06° per step and 100 s/step integration time. The obtained XRD patterns are analyzed using a Rietveld refinement method (Rietveld 1967, 1969) with the software MAUD (Lutterotti et al. 2004; Lutterotti 2010). An impactor is used to sample nanoparticles on carbon-coated TEM grids which were investigated with high-resolution transmission electron microscopy (Tecnai F20, FEI, Hillsboro, OR, USA) operating at 200 kV with 0.23 nm point resolution.

Model for the determination of crystal structure and carbon content of product powder by XRD

Produced TiC_XN_{1-X} powders were analyzed by means of XRD and the diffractograms were subjected to a Rietveld refinement analysis, yielding the lattice constant a. The model for the Rietveld refinement assumes a Ti-ordered and C–N-disordered NaCl FCC lattice, which was reported by Levi (Levi et al. 1998). Due to the small difference in the atomic form factor between N and C, it is impossible to use the peak intensities to fit the composition directly and a method using the lattice constant a is applied. In an investigation reporting the lattice constants for different C/N contents of commercial TiC_XN_{1-X} powders, an equation is given which allows to determine the lattice constant at different temperatures and values X indicating the C occupancy of the C–N sites (Aigner et al. 1994). This equation can be adapted to calculate X and following Vegard's law results for $T = 298$ K and for the valid range of the lattice constant $\boldsymbol{a}$ between $a = 4.239$ **Å** (TiN) and $a = 4.327$ **Å** (TiC) in a linear relation:

$$X = 11.437\,\frac{1}{\text{Å}} \times \text{a}[\text{Å}] - 48.484. \quad (1)$$

The peak positions yield the value of a and thereby X between 0 and 1, allowing to calculate the peak intensities for a given relative presence of C and N atoms at the C/N sites in the next step. In Fig. 3, some exemplary XRD patterns are shown for powders ranging from pure TiN via TiC_XN_{1-X} to pure TiC. It can be seen that the results from this refinement match very well the structural model for TiC_XN_{1-X} and the structural assumptions seem to be justified. It is important to note that the product is not a mixture of TiC and TiN powder, but a single-phase material. All powders show the same atomic structure and the substitution of C by N only leads to a shift in the lattice constant. Therefore, in the remaining of this work this method is used to determine the C occupancy of the C–N sites. The only minor impurities detected (at $2\theta = 32.1°$, $2\theta = 49.8°$, and $2\theta = 66.6°$) are attributed to WC (Leciejewicz 1961) as a result from erosion of the tungsten electrode. It is important to note that no oxide impurities by a TiO_X phase can be detected by XRD.

Results

In our experiments, we keep the electrical parameters of the anodic arc process constant and investigate the influence of the gas composition. First, we look on the production rate and then we focus on the particles composition and structure.

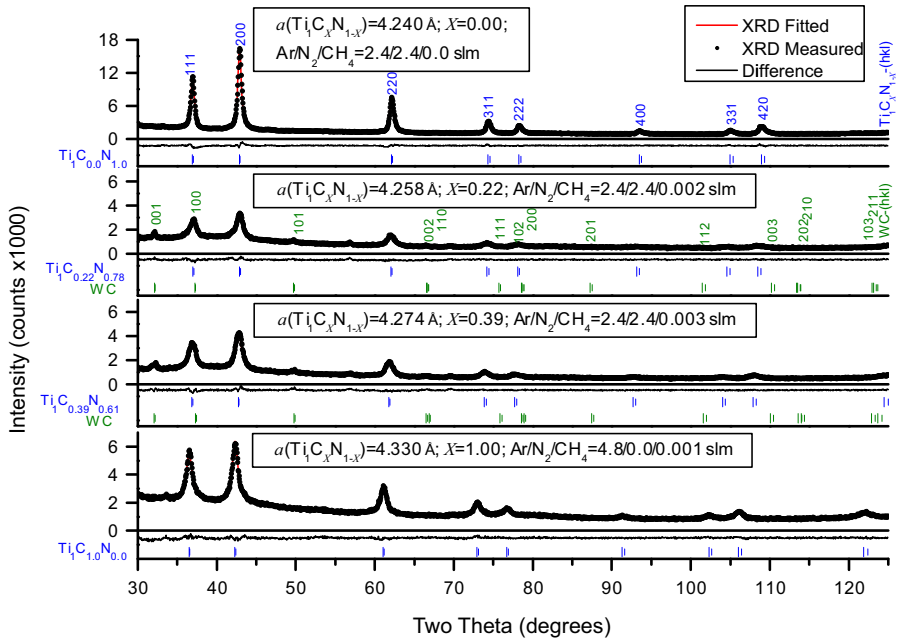

Fig. 3 Powder diffraction diagrams' results shown for four different product samples, where the composition was changed by variation of the content in the gas (caption indicates the $Ar/N_2/CH_4$ flow rates in slm). The C occupancy of the C–N sites *X* from TiC_XN_{1-X} was obtained from Eq. (1)

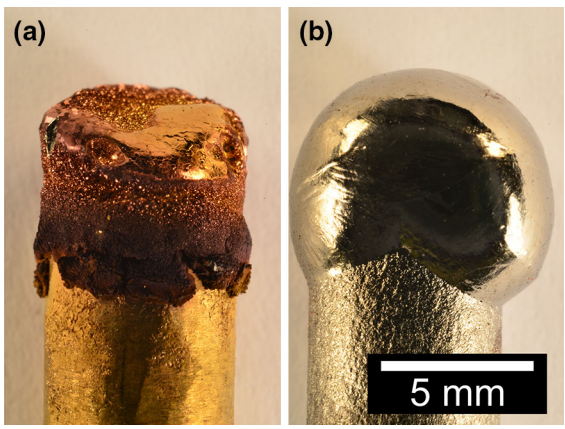

Fig. 4 Titanium electrodes (**a**) after being used in $Ar–N_2$ plasma (both with 2.4 slm), showing a golden-colored TiN surface with small 20–300 μm spots, (**b**) after being used in an $Ar-CH_4$ (4.8 slm and 1 sccm, respectively) plasma, leading to a large 9 mm Ti-ball at the top

Production rate

A change of the gas composition from Ar to N_2 has a large influence on the particle production rate of the plasma, whilst the small amount of CH_4 (only up to 0.06 vol%) added has no effect. A change of the gas composition influences the arc voltage and thus the consumed power which is slightly lower in the case of Ar. More importantly, it also has an influence on the structure of the titanium anode. Figure 4a shows a Ti anode which was used in an $Ar–N_2$ plasma, in Fig. 4b an $Ar–CH_4$ plasma is displayed. The first difference is the color which is golden in the $Ar–N_2$ case due to formation of titanium nitride by diffusion of nitrogen into the top layer of the anode, while the titanium anode used in $Ar–CH_4$ shows no color change from the grayish titanium color. Another difference is the size of the molten pools of titanium. In an $Ar–CH_4$ plasma, a large molten pool of Ti 6–9 mm in diameter forms, which leads to the spherical shape of the anode top after solidification. In the titanium nitride case, the melting temperature is 3220 K which is 1280 K higher than for pure Ti. Due to this higher melting point the electrode stays solid, however small pools in the size of a single spot (20–300 μm) form. This leads to an extremely high local temperature seen by brightly emitting small spots where the arc strikes the anode. When using nitrogen an appreciable mass transfer from the anode to the cathode in form of small titanium nitride, micron-sized particles can be recognized. This effect can lead to a short circuit between cathode and anode, which stops the particle production. Using pure N_2 this effect is more dominant than in an $Ar–N_2$ plasma and thus an $Ar–N_2$ plasma shows a longer stability before tuning is needed.

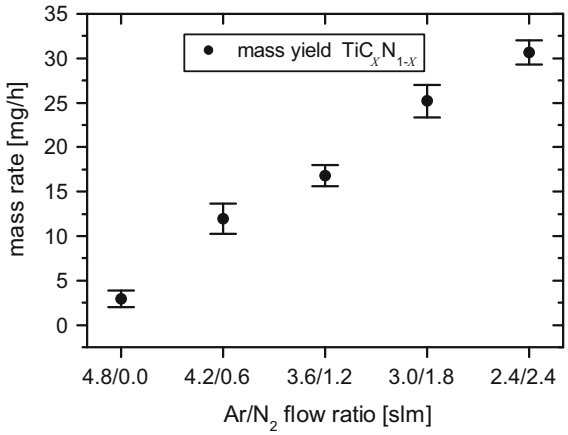

Fig. 5 Online measurements mean production rate as function of N_2 content in the gas mixture (including 1 sccm CH_4)

To determine the instantaneous production rate for a specific Ar–N_2 composition, an online measurement setup consisting of the dilution system and the TEOM measuring the mass concentration was used. Good time constancy can be achieved with nitrogen flow rates up to 2.4 slm, higher rates lead to the aforementioned electrode-short circuit. Note that the total flow rate of Ar and N_2 has been kept constant to 4.8 slm. The production rate was measured for 60 min to obtain the mean production rate as function of the gas composition (Fig. 5). As indicated by the error bars, small fluctuations in the order of ±2 mg/h have occurred during this time. They can be explained by small changes in the arc length and whether the attachment position is liquid or solid, as well as the

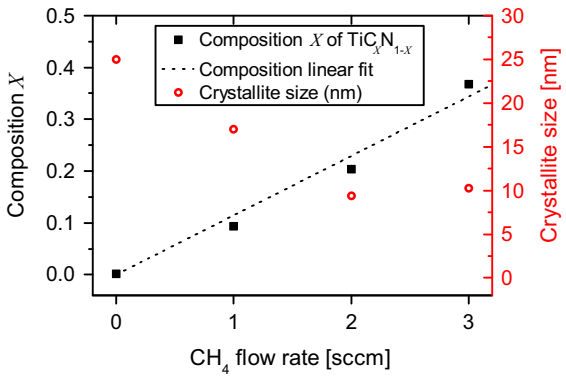

Fig. 6 C occupancy of the C–N sites (X) and crystallite size as function of methane flow, using 2.4 slm nitrogen and 2.4 slm argon

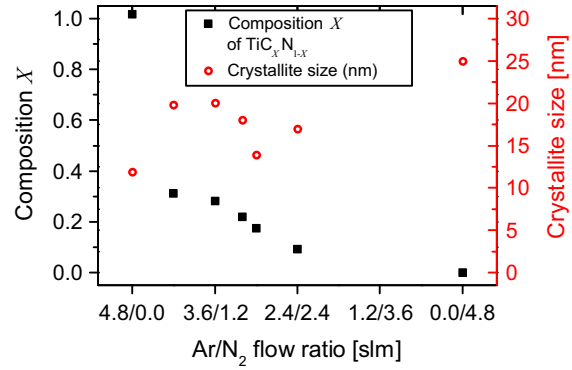

Fig. 7 C occupancy of the C–N sites (X) and crystallite size as function of the N_2 content of the gas mixture N_2–Ar with the methane flow kept constant at 1 sccm

noise in the TEOM signal due to the instruments adjustment mechanism of the oscillator frequency (remaining noise after a 1 min averaging procedure and no load: $\sigma = 0.5$mg/h). Here it can be seen, that by increasing the nitrogen content in the Ar/N_2/CH_4 gas mixture, the production rate strongly increases.

Particle composition

The composition and crystallite size is identified by XRD measurements. In a first set of experiments, the particles have been synthesized in a N_2/Ar gas mixture with a total flow rate of 4.8 slm and a N_2 content of 50 %. This assures a constant production rate. To change the composition, the flow rate of CH_4 and thus the available carbon is varied. Figure 6 shows the C occupancy of the C–N sites as determined by the method described in the experimental section. It can be seen that there exists an almost linear behavior between the CH_4 flow rate and the C occupancy. From Fig. 6, it can also be seen that crystallite size decreases with increasing CH_4 flow rate. At CH_4 flow rates much larger than 3 sccm, undesirable free carbon contamination was found.

In a second set of experiments, the product powder was synthesized with varying concentrations of N_2 in the N_2/Ar gas mixture with a flow rate of 4.8 slm, keeping the CH_4 flow rate and thus the available carbon constant (at 1 sccm). In Fig. 7, it can be seen that the C occupancy of the C–N sites decreases when the N_2 content increases. Without N_2, pure TiC is formed. When N_2 is added, TiC_XN_{1-X} is formed with a high carbon content in the particles. This can

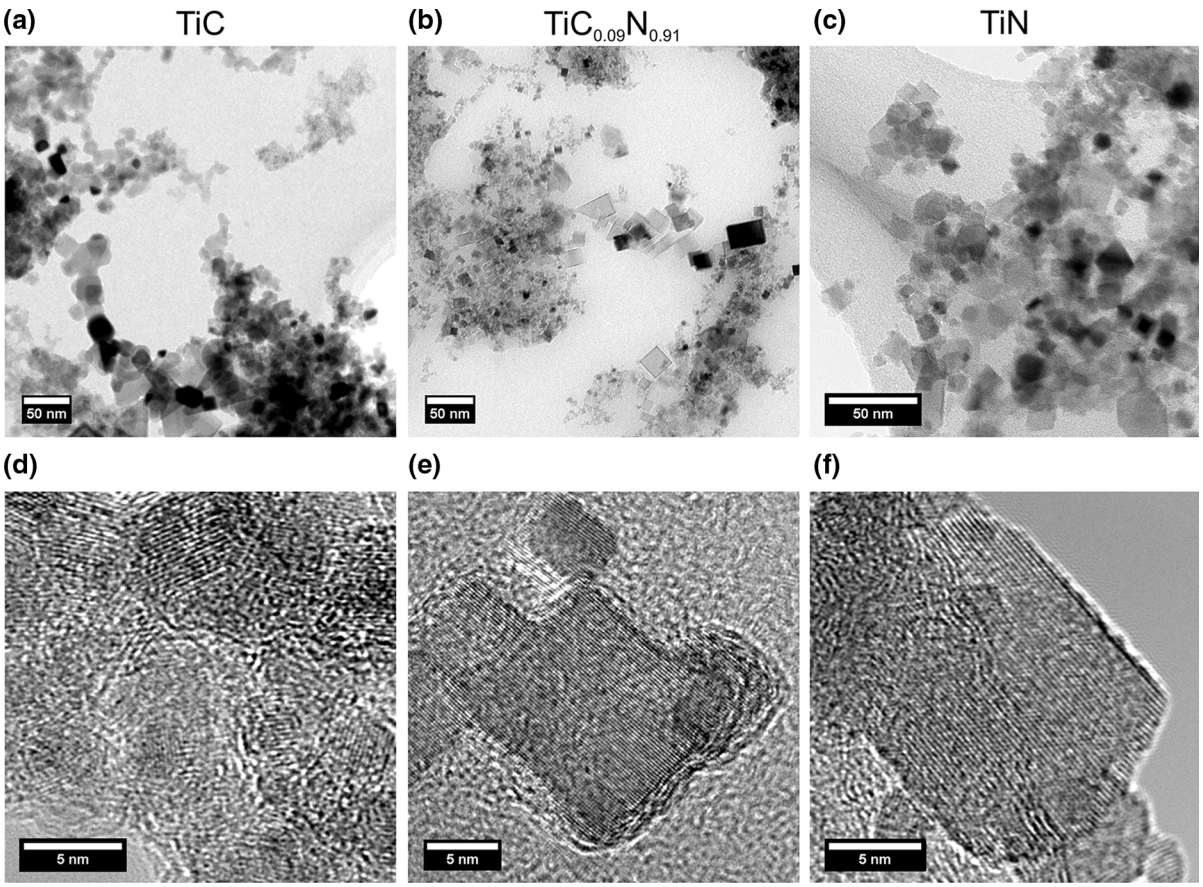

Fig. 8 TEM micrographs from *left* to *right* **a, d** TiC, **b, e** $TiC_{0.09}N_{0.91}$ to **c, f** TiN particles (see Table 3 samples (A),(D),(C), respectively). Parts **a** to **c** show an overview of size and shape, parts **d** to **f** show HR-TEM

exemplary be shown by the first step, where 0.6 slm N_2 compared to 0.001 slm CH_4 are added, which means that there is 1200 times more nitrogen than carbon available in the system. The composition of the particles formed is $TiC_{0.31}N_{0.69}$, which means only 2.2 times more nitrogen than carbon in the particles. Without the addition of Ar, nearly pure TiN forms. The crystallite size of the carbonitrides is between $\sim$15 and $\sim$25 nm, in between the values for pure TiC and pure TiN.

Particle morphology

The particle morphology is studied with help of HR-TEM micrographs. Pure TiN particles, synthesized in pure N_2 show a cubic habitus which is typical for a NaCl-type structure (Fig. 8c). Most particles are single crystalline, the particle size ranges from 4 to 40 nm. Pure TiC particles, produced in 4.8 slm Ar and 1 sccm CH_4, are slightly more aggregated and do not show this clear cubic habitus (Fig. 8a). It can be seen that the TiC sample shows a larger number of very small crystallites as compared to the TiN sample. This is in good agreement with the crystallite sizes for these systems as determined by means of XRD and shown in Fig. 7 ($\sim$10 nm for TiC and $\sim$25 nm for TiN).

Figure 8a of TiC shows many very fine particles which might be mistaken as amorphous structures. A further investigation with HR-TEM Fig. 8d shows that these regions consist of crystalline material of sizes around 3 nm. The corresponding lattice parameter obtained from the 2d-Fourier transformation can be attributed to TiC (hkl) (100) or (111) rocksalt structure.

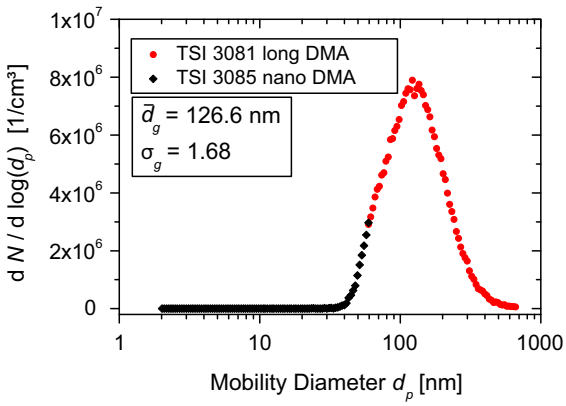

Fig. 9 Online measurement: aerosol number distribution obtained from SMPS using two different DMAs (N_2/Ar/CH_4 with 2.4/2.4/0.001 slm)

The HR-TEM micrographs of $TiC_{0.1}N_{0.9}$ particles [Fig. 8(b)] show similar cubic shape as in case of TiN. The cubic form is characteristic both for TiN as well as TiC and has been reported for TiC_XN_{1-X} as well (Grabis and Zalite 2005). Both large single crystalline grains as shown in Fig. 8e as well as very small, approximately 3 nm small single particles can be seen. The peaks of a 2d-Fourier transformation of Fig. 8e can be attributed to atomic layer periodicities in the fcc rocksalt structure of the TiC_XN_{1-X} phase, although the error is too large to identify the slight shift in the lattice constant and thus indentify the phase unambiguously as TiC $(a/2 = 2,16\,\text{Å})$, TiN $(a/2 = 2,12\,\text{Å})$, or TiC_XN_{1-X} (in between).

To determine the morphology of the particles in the gas phase when they leave the reactor, the diluted aerosol was also introduced into the SMPS for obtaining the aerosol number density distribution (Fig. 9). Using a gas composition N_2/Ar/CH_4 with 2.4/2.4/0.001 slm, a geometric mean diameter of 126.6 nm was determined. For other gas compositions, we see only a minor change by 20 nm. These diameters are much larger than the crystallite size as determined from XRD and the primary particles observed in TEM micrographs, of around 20 nm. It can be concluded that the product particles leave the process as agglomerates. This is due to coagulation occurring at high number concentrations. Two different DMAs were used in the SMPS in order to cover the full size range between 2 and 700 nm, especially to be able to detect the primary particle sizes; however, no single primary particles in the range around 20 nm were detected.

Discussion

Table 3 is summarizing the experimental findings. It can be seen that the production rate increases with the N_2 concentration in the carrier gas. An important change is that the titanium anode is altered by the nitrogen and thus changes the material to evaporate. This increase in production rate has been observed as well for changing Ar/N_2 mixtures by Tanaka et al. (1987) for Si/SiN and by Stein et al. (2013) for non nitride-forming metals (Cu, Ag, and Zn) in an arc. Their explanation is that additional energy is transferred from the plasma to the electrode when dissociated nitrogen atoms recombine at or within the electrode material, leading to a higher electrode temperature and bubble formation in contrast to the monoatomic Ar gas where no molecular recombination occurs. The increase of the production rate is accompanied by increasing crystallite size, due to increased mass density.

Our experiments show that composition of the particles is governed by the amount of carbon added into the system and not the N_2. When we compare sample (B) and (D) from Table 3, the carbon content has been kept constant and the nitrogen content is increased. The particles' composition changes from $TiC_{0.31}N_{0.69}$ to $TiC_{0.09}N_{0.91}$ containing only $\sim$1/3 of the carbon, but we can see also that the production rate nearly tripled. When we increase the available carbon now by a factor three [see sample (D) to (E)], the composition goes back to $TiC_{0.35}N_{0.65}$. Stoichiometric calculations show that all available carbon is included in the particles. This can be explained by the fact that TiC is thermodynamically more stable than TiN at high temperatures [above 1600 °C (Monteverde et al. 2001) or 1900 °C (Wang et al. 2005)]. So when the Ti-vapor is rapidly cooled down, all available C atoms will precipitate in the particles and occupy N sites of the TiN forming the carbonitride.

An interesting result from TEM is that TiC particles produced in pure Ar have a more spherical habitus than TiC_XN_{1-X} or TiN particles. A possible explanation can be given with the help of different behaviors of the Ti-electrodes. Figure 3 shows a smooth metallic Ti electrode when using 4.8 slm

Table 3 Synoptic table of the experimental results from XRD, TEOM, and TEM as function of the gas composition

	Conc. N_2 (vol %)	Conc. CH_4 (vol %)	Particle composition	Crystallite size (nm)	Production rate (mg/h)	Morphology
(A)	0.0	0.02	TiC	11.9	3	Aggregated spheres
(B)	12.5	0.02	$TiC_{0.31}N_{0.69}$	19.8	12	Aggregated cubes
(C)	50	0	$TiC_{0.001}N_{0.999}$	25.0	30	
(D)	50	0.02	$TiC_{0.09}N_{0.91}$	17.0		
(E)	50	0.06	$TiC_{0.35}N_{0.65}$	10.2		
(F)	100	0.02	$TiC_{0.001}N_{0.999}$	25.0	(Unstable) 70	

The total flow rate of N_2 + Ar is 4.8 slm

Ar + 1 sccm CH_4 from the production of TiC and a rough electrode with a TiN surface coating when using 2.4 slm Ar + 2.4 slm N_2 to produce TiC_XN_{1-X}. The much larger concentration of reactant in case of TiN leads to direct nitridation of the electrode and subsequent evaporation of TiN molecules, followed by a direct nucleation and growth of strongly faceted TiN crystals. In case of TiC, the titanium electrode directly evaporates and the TiC is formed at much lower concentrations of the reactant (1 sccm CH4 vs. 2.4 slm N_2). The lower concentration can lead to slower formation of the solid product and a longer lifetime of the titanium in form of small metallic droplets. The intermediate presence of a liquid phase may explain the more spherical shapes of the TiC particles, as opposed to the clear crystalline form of the TiN particles. The existence of a liquid TiC phase for a stoichiometric Ti to C ratio in the presence of H_2 and Ar in a plasma is also predicted by phase calculations published by Ishigaki et al. (Ishigaki et al. 1996), while they predict in the same paper a sublimation–resublimation mechanism for TiN in the presence of an excess of nitrogen in the plasma.

Conclusions

A synthesis process has been developed yielding TiC, TiN, and TiC_XN_{1-X} nanoparticles which are compatible with a commercial PVD coating system. This is obtained with a relatively simple and low-cost nanoparticle generator, in contrast to the conventionally used DC or RF plasma torches, based on a DC anode evaporation system with a TIG-welding power supply. It has a stable production rate over an extended time period (several hours) and does not require corrosive or expensive chemical precursors. The process shows a nanoparticle production rate from 5 to 30 mg/hr at a constant total gas flow rate of 4.8 slm. The produced nanoparticles have crystallite sizes between 8 and 27 nm, some samples containing even finer particles around 3 nm. The particles are single crystalline, cubic particles indicating a possible vapor to solid condensation mechanism.

The synthesis of the titanium carbonitride in nanoparticulate form is scarcely reported. Therefore, an extensive study is made into the effect of the composition of the plasma gases, which are N_2 and Ar for synthesizing TiN, Ar, and CH_4 for synthesizing TiC, and mixtures thereof for synthesizing TiC_XN_{1-X}. The composition obtained is expressed in form of the carbon occupancy of the C–N sites, and is determined from XRD analysis of the lattice parameter. An almost linear behavior between the CH_4 flow rate and the C occupancy has been found. This can be explained by the fact that TiC is thermodynamically more stable than TiN at high temperatures, so that all available C atoms will precipitate in the particles and occupy N sites of the TiN forming the carbonitride. For this reason, the flow rate of the CH_4 required to obtain only a partial occupancy of the C–N sites by C has to be such that there are more Ti atoms evaporated than C atoms originating from the CH_4. In the present reactor, this leads to typical flow rates of a few sccm CH_4 as compared to several slm N_2; too large CH_4 concentrations lead to undesirable free carbon contamination.

Acknowledgments This work was financially supported by the Deutsche Forschungsgemeinschaft (DFG) in the framework of the Collaborative Research Centre on "Nanoparticles from the gas phase: formation, structure and properties" (SFB 445).

References

Aigner K, Lengauer W, Rafaja D, Ettmayer P (1994) Lattice parameters and thermal expansion of $Ti(C_xN_{1-x})$, $Zr(C_xN_{1-x})$, $Hf(C_xN_{1-x})$ and TiN_{1-x} from 298 to 1473 K as investigated by high-temperature X-ray diffraction. J Alloy Compd 215(1–2):121–126. doi:10.1016/0925-8388(94)90828-1

Alekseev NV, Samokhin AV, Tsvetkov YV (1999) Synthesis of titanium carbonitride nanopowder by titanium tetrachloride treatment in hydrocarbon-air plasma. High Energy Chem 33(3):194–197

Alexandrescu R, Borsella E, Botti S, Cesile MC, Martelli S, Giorgi R, Turtù S, Zappa G (1997) Synthesis of TiC and SiC/TiC nanocrystalline powders by gas-phase laser-induced reaction. J Mater Sci 32(21):5629–5635. doi:10.1023/A:1018640911556

EFSA Panel on food contact materials enzymes (CEF) (2012) Scientific opinion on the safety evaluation of the substance, titanium nitride, nanoparticles, for use in food contact materials. EFSA J 10(3):2641–2649. doi:10.2903/j.efsa.2012.2641

Feng X, Shi L (2005) Facile synthesis of nanocrystalline titanium carbonitride via a chemical metathesis route. Chem Lett 34(7):1002–1003. doi:10.1246/cl.2005.1002

Grabis J, Zalite I (2005) Preparation of Ti (N, C) based nanosized powders and their densification. Mater Sci 11(4): 372–375

Guu YY, Lin JF, Ai C (1997) The tribological characteristics of titanium nitride, titanium carbonitride and titanium carbide coatings. Thin Solid Films 302(1–2):193–200. doi:10.1016/S0040-6090(96)09546-6

Ikegami A, Kimura Y, Suzuki H, Sato T, Tanigaki T, Kido O, Kurumada M, Saito Y, Kaito C (2003) Growth process of TiC clusters from Ti nanoparticles with evaporated carbon layer. Surf Sci 540(2–3):395–400. doi:10.1016/S0039-6028(03)00875-6

Inoue A, Kim BG, Nosaki K, Yamaguchi T, Masumoto T (1992) Production of a TiN film with nanoscale particle size by a combined method of plasma-alloy reaction and spray deposition. J Mater Sci Lett 11(12):865–867. doi:10.1007/BF00730489

Ishigaki T, Sato T, Moriyoshi Y, Boulos MI (1995) Influence of plasma modification of titanium carbide powder on its sintering properties. J Mater Sci Lett 14(23):1694–1697. doi:10.1007/BF00422678

Ishigaki T, Moriyoshi Y, Watanabe T, Kanzawa A (1996) Thermal plasma treatment of titanium carbide powders: part II. In-flight formation of carbon-site vacancies and subsequent nitridation in titanium carbide powders during induction plasma treatment. J Mater Res 11(11):2811–2824. doi:10.1557/JMR.1996.0356

Ishizaki K, Egashira T, Tanaka K, Celis PB (1989) Direct production of ultra-fine nitrides (Si_3N_4 and AIN) and carbides (SiC, WC and TiC) powders by the arc plasma method. J Mater Sci 24(10):3553–3559. doi:10.1007/BF02385739

Iwama S, Hayakawa K, Arizumi T (1982) Ultrafine powders of TiN and AlN produced by a reactive gas evaporation technique with electron beam heating. J Cryst Growth 56(2):265–269. doi:10.1016/0022-0248(82)90443-2

Jhi S, Ihm J, Loule SG, Cohen ML (1999) Electronic mechanism of hardness enhancement in transition-metal carbonitrides. Nature 399(6732):132–134. doi:10.1038/20148

Jiao J, Seraphin S (1998) Carbon encapsulated nanoparticles of Ni Co, Cu, and Ti. J Appl Phys 83(5):2442–2448. doi:10.1063/1.367004

Leciejewicz J (1961) A note on the structure of tungsten carbide. Acta Cryst 14(2):200. doi:10.1107/S0365110X6100067X

Leconte Y, Maskrot H, Herlin-Boime N, Porterat D, Reynaud C, Gierlotka S, Swiderska-Sroda A, Vicens J (2006) TiC nanocrystal formation from carburization of laser-grown Ti/O/C nanopowders for nanostructured ceramics. J Phys Chem B 110(1):158–163. doi:10.1021/jp054471p

Lee D, Ahn J, Chung H (2007) Synthesis and nitrogen stability of ultrafine titanium carbonitride particles. J Mater Res 22(01):233–237. doi:10.1557/jmr.2007.0024

Leparoux M, Kihn Y, Paris S, Schreuders C (2008) Microstructure analysis of RF plasma synthesized TiCN nanopowders. Int J Refract Met H 26(4):277–285. doi:10.1016/j.ijrmhm.2007.06.003

Levi G, Kaplan WD, Bamberger M (1998) Structure refinement of titanium carbonitride (TiCN). Mater Lett 35(5–6):344–350. doi:10.1016/S0167-577X(97)00276-0

Li Y, Yao Y, Shao W, Liu F, Kang Y, Yin G, Huang Z, Liao X (2009) Preparation of titanium carbonitride nanoparticles from a novel refluxing-derived precursor. Mater Lett 63(22):1904–1906. doi:10.1016/j.matlet.2009.05.031

Lutterotti L (2010) Total pattern fitting for the combined size–strain–stress–texture determination in thin film diffraction. X-ray techniques for advanced materials, nanostructures and thin films: from laboratory sources to synchrotron radiation. In: Proceedings of the EMRS 2009 Spring Meeting—Symposium R 268(3–4):334–340. doi: 10.1016/j.nimb.2009.09.053

Lutterotti L, Chateigner D, Ferrari S, Ricote J (2004) Texture, residual stress and structural analysis of thin films using a combined X-ray analysis. In: Proceedings of symposium m on optical and x-ray metrology for advanced device materials characterization, of the E-MRS 2003 Spring Conference 450(1):34–41. doi: 10.1016/j.tsf.2003.10.150

Mahoney W, Andres RP (1995) Aerosol synthesis of nanoscale clusters using atmospheric arc evaporation. Mater Sci Eng A 204(1–2):160–164. doi:10.1016/0921-5093(95)09953-0

Manoj Kumar BV, Basu B, Vizintin J, Kalin M (2008) Tribochemistry in sliding wear of TiCN-Ni-based cermets. J Mater Res 23(5):1214–1227. doi:10.1557/jmr.2008.0165

Mehta P, Singh AK, Kingon AI (1991) Nonthermal microwave plasma synthesis of crystalline titanium oxide and titanium nitride nanoparticles. MRS Proc 249:153–158. doi:10.1557/PROC-249-153

Mitrofanov B, Mazza A, Pfender E, Ronsheim P, Toth LE (1981) D.C. arc plasma titanium and vanadium compound synthesis from metal powders and gas phase non-metals. Mater Sci Eng 48(1):21–26. doi:10.1016/0025-5416(81)90062-8

Mondal B, Das P, Singh S (2008) Advanced WC–Co cermet composites with reinforcement of TiCN prepared by extended thermal plasma route. Mater Sci Eng A 498(1–2):59–64. doi:10.1016/j.msea.2007.10.127

Monteverde F, Medri V, Bellosi A (2001) Synthesis of ultrafine titanium carbonitride powders. Appl Organomet Chem 15(5):421–429. doi:10.1002/aoc.164

Mu Y, Wang M, Yu D (2011) Synthesis of Ti(CN) powders by combustion reaction from Ti powder and a novel carbon–nitrogen precursor. Int J Refract Met H 29(2):326–328. doi:10.1016/j.ijrmhm.2010.10.001

Pfender E (1999) Thermal plasma technology: where do we stand and where are we going? Plasma Chem Plasma Proc 19(1):1–31. doi:10.1023/A:1021899731587

Rietveld H (1967) Line profiles of neutron powder-diffraction peaks for structure refinement. Acta Crystallogr 22(1): 151–152. doi:10.1107/S0365110X67000234

Rietveld H (1969) A profile refinement method for nuclear and magnetic structures. J Appl Crystallogr 2(2):65–71. doi:10.1107/S0021889869006558

Seplyarskii BS, Brauer GB, Tarasov AG (2011) Combustion of the gasless system Ti + 0.5C in a nitrogen coflow. Combust Explos Shock 47(3):294–301. doi:10.1134/S0010508211030063

Shen G, Tang K, An C, Yang Q, Wang C, Qian Y (2002) A simple route to prepare nanocrystalline titanium carbonitride. Mater Res Bull 37(6):1207–1211. doi:10.1016/S0025-5408(02)00736-5

Stein M, Kiesler D, Kruis FE (2013) Effect of carrier gas composition on transferred arc metal nanoparticle synthesis. J Nanopart Res 15(1):1–14. doi:10.1007/s11051-012-1400-9

Tanaka K, Ishizaki K, Yumoto S, Egashira T, Uda M (1987) Production of ultra-fine silicon powder by the arc plasma method. J Mater Sci 22(6):2192–2198. doi:10.1007/s11051-012-1400-9

Thompson GS, Harmer MP (2011) Nanoscale ceramic composites. In: Buschow KHJ, Cahn RW, Flemings MC, Ilschner B, Kramer EJ, Mahajan S, Veyssière P (eds) Encyclopedia of materials: science and technology, 2nd edn. Elsevier, Oxford, pp 5927–5930

Wang Y, Chen K, Zhou H (2005) Combustion synthesis of Ti(C,N) powder. Key Eng Mat 280–283:1421–1424. doi:10.4028/www.scientific.net/KEM.280-283.1421

Yang Q, Lengauer W, Koch T, Scheerer M, Smid I (2000) Hardness and elastic properties of $Ti(C_xN_{1-x})$, $Zr(C_xN_{1-x})$ and $Hf(C_xN_{1-x})$. J Alloy Compd 309(1–2):L5. doi:10.1016/S0925-8388(00)01057-4

Yatsui K, Grigoriu C, Masugata K, Jiang W, Sonegawa T (1997) Preparation of thin films and nanosize powders by intense, pulsed ion beam evaporation. Jpn J Appl Phys 1 36(7 SUPPL. B):4928–4934. doi:10.1143/JJAP.36.4928

Yeh C, Chen Y (2005) Direct formation of titanium carbonitrides by SHS in nitrogen. Ceram Int 31(5):719–729. doi:10.1016/j.ceramint.2004.07.013

Yin F, Zhou L, Xu Z, Xue B, Jiang X (2009) Synthesis of nanocrystalline titanium carbonitride during milling of titanium and carbon in nitrogen atmosphere. J Alloy Compd 470(1–2):369–374. doi:10.1016/j.jallcom.2008.02.073

Young RM, Pfender E (1985) Generation and behavior of fine particles in thermal plasmas-A review. Plasma Chem Plasma Process 5(1):1–37. doi:10.1007/BF00567907

Zhang JP, Shi LY, Feng X (2008) Low pressure pyrolysis of melamine: novel route to preparing titanium carbonitride nanocrystals. Mater Technol 23(3):158–160. doi:10.1179/175355508X310197